AIP | The Journal of Chemical Physics

A multi-agent quantum Monte Carlo model for charge transport: Application to organic field-effect transistors

Thilo Bauer, Christof M. Jäger, Meredith J. T. Jordan, and Timothy Clark

Citation: The Journal of Chemical Physics **143**, 044114 (2015); doi: 10.1063/1.4927397
View online: http://dx.doi.org/10.1063/1.4927397
View Table of Contents: http://scitation.aip.org/content/aip/journal/jcp/143/4?ver=pdfcov
Published by the AIP Publishing

A multi-agent quantum Monte Carlo model for charge transport: Application to organic field-effect transistors

Thilo Bauer,[1] Christof M. Jäger,[1,a)] Meredith J. T. Jordan,[2] and Timothy Clark[1,3,b)]
[1]*Department of Chemistry and Pharmacy, Computer-Chemistry-Center and Interdisciplinary Center for Molecular Materials, Friedrich-Alexander-Universität Erlangen-Nürnberg, Nägelsbachstrasse 25, 91052 Erlangen, Germany*
[2]*School of Chemistry, University of Sydney, Sydney, NSW 2006, Australia*
[3]*Centre for Molecular Design, University of Portsmouth, Portsmouth PO1 2DY, United Kingdom*

(Received 13 May 2015; accepted 13 July 2015; published online 29 July 2015)

We have developed a multi-agent quantum Monte Carlo model to describe the spatial dynamics of multiple majority charge carriers during conduction of electric current in the channel of organic field-effect transistors. The charge carriers are treated by a neglect of diatomic differential overlap Hamiltonian using a lattice of hydrogen-like basis functions. The local ionization energy and local electron affinity defined previously map the bulk structure of the transistor channel to external potentials for the simulations of electron- and hole-conduction, respectively. The model is designed without a specific charge-transport mechanism like hopping- or band-transport in mind and does not arbitrarily localize charge. An electrode model allows dynamic injection and depletion of charge carriers according to source-drain voltage. The field-effect is modeled by using the source-gate voltage in a Metropolis-like acceptance criterion. Although the current cannot be calculated because the simulations have no time axis, using the number of Monte Carlo moves as pseudo-time gives results that resemble experimental I/V curves. [http://dx.doi.org/10.1063/1.4927397]

I. INTRODUCTION

Charge transport in organic semiconductors (OSCs) with an amorphous structure is usually described using the concept of hopping-transport.[1] Depending on the amount of disorder in the structure, the concept of band-like transport is also discussed as a borderline case in the limit to band structures in well-ordered crystalline systems.[2,3] For higher temperatures and strong electron-phonon-coupling,[2] the hopping rate or frequency is derived from Marcus theory,[4] for lower temperatures and weak electron-phonon-coupling from the Miller-Abrahams model.[1,5] Although these approaches can be quite successful, they suffer, for instance, from ambiguities in the definition of the attempt-to-hop rate in the Miller-Abrahams model and the transfer integral in Marcus theory.[2] Some approaches model the transport of only single charge carriers,[2,3] making it difficult to describe changes in transport characteristics caused by trapping.

The molecular structure of the channel of organic field-effect transistors (OFETs) made from self-assembled monolayers can be considered to be largely amorphous,[6–10] but regions of higher order are also observed.[11–13] Molecular structures that are as close to real world situations as possible must be used to account for such complex molecular environments. An adequate charge transport model must therefore account for the effects of static and dynamic disorders naturally. Single molecules and non-bulk geometries represent far too severe approximations for such cases. Furthermore, if the model is to allow direct comparisons between different OSC systems, the approximations and methods used must be independent of the systems investigated (i.e., they must be as universally applicable as possible).

Multi-agent modeling has become a useful tool for investigating systems consisting of entities with defined or definable characteristics. Key to this concept is that the entities act autonomously based on diverging interests and/or different information. Systems that can be modeled in this way are called multi-agent systems (MASs) and the entities agents. The concept of an agent is not defined beyond the very basic requirements of autonomy, possible information disparity, and diverging goals or interests; they may be anything from traders in stock markets,[14] cars, trains, or airplanes in traffic,[15] or humans in organizations[16] to computer systems in software engineering.[17] Basically, MAS modeling is the simulation tool of choice for learning about the structure and dynamics of the system's processes from the behavior of its constituting agents, i.e., when the processes need to be a result of and not an input to the model.

We present here a charge-transport model based on a Monte Carlo approach, in which charge carriers are represented by multiple quantum mechanical agents on a local energy hypersurface. This model does not require a specific charge-transport mechanism as prerequisite, but rather delivers the mechanism as a result of its application. It is capable of describing the spatial distribution of multiple charge carriers during conduction of electric current in complete devices and covers both static and dynamic disorders by design.

a)Current address: Department of Chemical and Environmental Engineering, University of Nottingham, University Park, Nottingham NG7 2RD, United Kingdom.
b)Author to whom correspondence should be addressed. Electronic mail: tim.clark@fau.de

II. METHODS

A. Local energy hypersurfaces

Hypersurfaces based on local energy properties $E_L(\mathbf{r})$ can describe the position-dependent electronic properties of matter such as the energetic effect of donating or accepting charge in specific regions.[18] The corresponding local energy property is either the local ionization energy, i.e., $E_L(\mathbf{r}) = I_L(\mathbf{r})$[19,20] or the local electron affinity, i.e., $E_L(\mathbf{r}) = A_L(\mathbf{r})$.[21,22] The two are defined as

$$I_L(\mathbf{r}) = \frac{-\sum_{i=1}^{HOMO} \varepsilon_i \rho_i(\mathbf{r})}{\sum_{i=1}^{HOMO} \rho_i(\mathbf{r})} \tag{1}$$

and

$$A_L(\mathbf{r}) = \frac{-\sum_{i=LUMO}^{Norbs} \delta_i \varepsilon_i \rho_i(\mathbf{r})}{\sum_{i=LUMO}^{Norbs} \delta_i \rho_i(\mathbf{r})}, \tag{2}$$

where *HOMO* is the highest occupied molecular orbital, *LUMO* is the lowest unoccupied, and *Norbs* the total number of orbitals. ε_i is the eigenvalue or orbital i, $\rho_i(\mathbf{r})$ is the electron density at position $\mathbf{r}$ attributable to molecular orbital i, and δ_i is a switching variable defined using the intensity-filtering technique.[20] $I_L(\mathbf{r})$ and $A_L(\mathbf{r})$ provide a spatially resolved description of the electron donating and accepting properties of a system and are thus well suited for describing electric conduction in p-type or n-type semiconductors, respectively. We have used these properties previously to visualize[23] and search[7] for charge-transport paths and have now found[24] them also to be useful in quantitative calculations of electron- and hole-mobilities. Conceptually, they correspond approximately to a one-electron description of the local energies of charge carriers. Although the equivalent of Koopmans' theorem for electron affinities is a very crude approximation, it is justifiable in this case as the effects of both the neglect of diatomic differential overlap (NDDO) approximation and the minimal basis set become less important for large systems such as the ones considered here. $I_L(\mathbf{r})$ hypersurfaces provide the external potential for holes in p-type semiconductors, while $A_L(\mathbf{r})$ hypersurfaces fulfill the same function for excess electrons in n-type semiconductors. Thus, the two local properties can be used as external potentials to explore the spatial dynamics of conduction by multiple majority charge carriers. The bulk electronic properties of devices can be linked to structural properties of the OFET channel and the chemical properties of the molecules from which it is assembled.

Local energy hypersurfaces are calculated as individual values associated with points on spatial grids that span the space of a molecular structure. The distance between neighboring grid points defines the resolution of the hypersurface and the quantum chemical information contained.

A proper description of the spatial dynamics must include aspects of device operation such as applied voltages, electrode geometries and materials, and charge carrier injection and interactions between charge carriers. To achieve this, we represent charge carriers as agents. The agents operate on the relevant hypersurface subject to physical constraints that capture interactions between charge carriers and applied potentials. The multi-agent paradigm then allows for an effective electrode model including injection.

Though the application of our method presented in Section II C focuses on the use of $E_L(\mathbf{r}) = A_L(\mathbf{r})$, the following description of the method is kept general to emphasize its applicability to both $A_L(\mathbf{r})$ and $I_L(\mathbf{r})$ hypersurfaces, i.e., electron- and hole-conduction.

B. Charge-carrier-multi-agent-paradigm (diffusion quantum Monte Carlo)

Agents are entities with a domain D of states to occupy and defined constraints and interactions between each other. Actions from a corresponding action vector are available to the agents to solve a given problem in order to occupy states from their domain within the defined constraints.

In the multi-agent paradigm, a charge carrier ψ_i (electron or hole) in a system of N electric charges is represented by a set of K agents ϕ_μ. Each agent represents a hydrogen $1s$-function located on the spatial grid used to calculate the E_L hypersurface. The agents are treated as basis functions with equal weight in a linear combination of atomic orbitals (LCAOs) approximation (Equation (3)) that leads to a limited-resolution charge carrier wavefunction determined by the Monte Carlo technique,

$$\begin{aligned} \psi_i &= \sum_{\mu=1}^{K} c_{\mu i} \phi_\mu, \\ c_{\mu i} &= \sqrt{\frac{1}{K}}. \end{aligned} \tag{3}$$

Agents of the same set as ϕ_μ are called supporting agents (ν), whereas agents of all sets representing different charge carriers are referred to as opposing agents (λ).

The domain D of an agent ϕ_μ is the set of all grid points of the simulation space C_{sim}, which is a subspace of the local-energy hypersurface grid. The set A of actions a that an agent at grid point $\mathbf{r}_\mu$ can take to improve its state is defined by its probability of moving to one of its 26 nearest neighboring grid points. Movements backwards or forwards in each spatial direction or no movement are possible, thus defining the set A_m of one-dimensional actions. An action a then is a triple of the cubic Cartesian product of A_m that forms A,

$$\begin{aligned} A_m &= \{-1, 0, 1\}, \\ A &= A_m^3 \\ &= \{(a_1, a_2, a_3) \,|\, a_i \in A_m \text{ for } i = 1, 2, 3\}, \\ a &\in A. \end{aligned} \tag{4}$$

The probability $P\left(\mathbf{r}_\mu, a, \mathbf{r}'_\mu\right)$ of ending on a neighboring grid point $\mathbf{r}'_\mu$ due to action a is specified by the *energetic reward* f_1 of occupying the respective state. f_1 is dependent on the local energy hypersurface and the positions $\mathbf{r}_{\nu,\lambda}$ of all supporting and opposing agents,

$$P : A \to f_1. \tag{5}$$

The probabilities are distributed via ℓ, which combines the probabilities $p = 1/27$ of randomly taking one of the 27 possible actions on the cubic grid and the probability q of accepting the chosen action subject to physical constraints,

$$\ell = \left[p : \left[q_1 : \mathbf{r}'_{\mu_1}\right], \ldots p : \left[q_{14} : \mathbf{r}'_{\mu_{14}} = \mathbf{r}_\mu\right], \ldots p : \left[q_{27} : \mathbf{r}'_{\mu_{27}}\right]\right]. \tag{6}$$

The non-heuristic nature of the agents does not allow them to act without additional information about their environment, which can only be gained by probing a new position. Thus, the action of deliberately staying in the current position is not valid and the triple $a_{14} = (0,0,0)$ is omitted. It follows that in A, there exist 26 valid actions for an agent with a position in the lattice bulk, 17 on a domain surface, 11 on a domain edge, and 7 at a vertex. This is formally expressed by the four sub-distributions $\ell_{26}, \ell_{17}, \ell_{11}, \ell_7$, in which q_{14} and the corresponding probabilities q_k for leaving the domain are set to zero.

In the technical implementation, actions are generated from random real numbers of the interval $[0,1)$, so that it is well possible that invalid moves are generated, even a_{14} for ℓ_{26}. The chance of invalid actions increases at the domain borders; so to avoid artificial "friction," agents need to carry out the same number of valid actions on average, regardless of their position. Multiple choices of actions from A are therefore allowed until a valid action, given by $\mathbf{r}'_\mu \in D \wedge \mathbf{r}'_\mu = \mathbf{r}_\mu$, is returned.

Constraints are introduced implicitly from the agents' interactions. On the one hand, these interactions must reproduce quantum mechanical properties of the charge carriers; on the other hand, they must allow for concerted interactions if multiple agents represent one physical charge carrier. Both types of interaction are included in our NDDO-like Hamiltonian F_2 (Equation (7)). The total energies f_2 calculated with F_2 are subsequently used to constrain the actions of the agents. Starting from a position $\mathbf{r}_\mu$, an agent takes random action a to move to a new position $\mathbf{r}'_\mu$ on one of its next neighboring grid points. Note that it is possible for multiple agents to occupy the same grid point, whether they are supporting or opposing. The energetic reward f_1 for action a as used in Equation (5) is then dependent on the difference of the total energies at the old (f_2) and new (f'_2) positions.

The total energy of an agent can be written as a sum of three terms; the first and second reproduce physical properties of the charge carriers while the third is due entirely to the multi-agent model. Note that in Equation (7), the parameters ρ_0^{H} for the Coulomb-interaction and β_s^{H} for the resonance integral, respectively, are scaled to the number of agents representing a single charge carrier,

$$F_2 = U_{\mu\mu} + \sum_{j=1, j\neq i}^{N} \sum_{\lambda=1}^{K} \frac{\left(\frac{1}{K}\right)^2}{\sqrt{d_{\mu\lambda}^2 + 4\left(\frac{\rho_0^H}{K}\right)^2}} + \sum_{\nu=1, \nu\neq\mu}^{K} S_{\mu\nu} \frac{\beta_s^H}{K}. \tag{7}$$

The first term of Equation (7), $U_{\mu\mu}$, represents the external potential, which is identical with the value of the local energy (I_L or A_L) at the agent's current position $\mathbf{r}_\mu$. Depending on the type of the OSC under investigation (n-type or p-type), $U_{\mu\mu}$ is either represented by A_L or I_L. As a high local electron-affinity corresponds with energetically more favorable positions, the negative of the local energy is used in F_2 in the former case, whereas in the latter case, energetically more favorable positions correspond to low local ionization energies,

$$U_{\mu\mu} = \begin{cases} -E_L(\mathbf{r}_\mu), E_L = A_L \\ E_L(\mathbf{r}_\mu), E_L = I_L \end{cases}. \tag{8}$$

The second term describes the Coulomb repulsion between agents that represent different charges. As an agent is an isotropic hydrogen *1s*-function, we can describe this repulsive interaction via the modified neglect of diatomic overlap (MNDO)-type monopole-interaction, in which $d_{\mu\lambda}$ represents the distance between agents and ρ_0^H is the Coulomb-interaction parameter for hydrogen.[28,29] Note that in Equation (9), the elementary charge and the parameter are scaled to the number of agents representing one physical charge carrier,

$$(\mu|\lambda) = \frac{\left(\frac{1}{K}\right)^2}{\sqrt{d_{\mu\lambda}^2 + 4\left(\frac{\rho_0^H}{K}\right)^2}}. \tag{9}$$

The third term describes an attractive interaction between agents representing the same charge carrier. This attractive interaction is necessary as the agents representing a physical charge must act in a concerted and supportive manner in order to find a Markov chain through space. We use the MNDO-resonance-integral[30] $\beta_{\mu\nu}$ to model this interaction, in which β_s^H is a parameter scaled to the number of agents representing one physical charge carrier.[29] This corresponds to a standard MNDO-like LCAO approximation for the construction of charge carriers from basis functions centered at different locations, as implicit in Equation (3),

$$\beta_{\mu\nu} = S_{\mu\nu} \frac{\beta_s^H}{K}. \tag{10}$$

The expression $S_{\mu\nu}$ in Equation (10) is the overlap between agents ϕ_μ and ϕ_ν. With standard parameters[29,31] for the hydrogen $1s$-function, the overlap between agents decreases too steeply with distance. Agents of a same charge carrier need to be able to communicate with each other over large distances in our systems. To enable the agents to act concertedly, we use a smaller Slater exponent ζ in the agent wavefunctions than in the original hydrogen functions,

$$\zeta = \frac{\zeta_{MNDO}^H}{8} = 0.166\,495\,875\ \mathrm{bohr}^{-1}. \tag{11}$$

Agents do not learn about their environment, i.e., they possess no information about the local energy hypersurface apart from their current position. They obtain temporary additional information only by taking an action a. Thus, while agents move to maximize their energetic reward from the set R of all grid points accessible via action a, the optimal action, i.e., $\left\{\mathbf{r}'_\mu | \max f_1\right\}$ is unknown. Therefore, the choice of actions is random and there is a non-zero probability of agents stepping to a grid point with higher energy, i.e., where $f'_2 > f_2$ and $f_1 \to 0$. Since the probability q of occupying positions $\left\{\mathbf{r}'_\mu \in R | f_1 < 1\right\} \Rightarrow f'_2 > f_2$ is $q < 1$, an acceptance criterion for such actions must be defined such that it not only uses the ratio of the total energies but also takes the agents' *ability to*

act into account. In the framework of field-effect transistors, the ability to act is largely given by the applied source-gate-voltage U_{GS}, so any acceptance criterion must reflect the effect of U_{GS} on the agents, and thus on the charge carriers.

We therefore define the action of occupying energetically higher states at grid points $\left\{\mathbf{r}'_\mu \in R \,|f'_2 > f_2\right\}$ to be allowed[32] with probability f_3, in which e is the elementary charge and $e\,|U_{GS}|$ is the field effect,

$$f_3 = \exp\left(-\frac{f'_2 - f_2}{e\,|U_{GS}|}\right). \tag{12}$$

For all states $\left\{\mathbf{r}'_\mu \,|f'_2 \le f_2\right\} = D^-$, function f_1 becomes $f_1\left(\mathbf{r}'_\mu\right) = 1$. For states $\left\{\mathbf{r}'_\mu \,|f'_2 > f_2\right\} = D^+$, the value of function f_1 depends on probability f_3 (see Appendix A 1).

In the technical implementation, the decision whether to accept the action is made by calculating a random number $n_r \in \mathbb{R}$ from $[0,1)$ which must be an element of $[0, f_3)$ in order to accept the action. Moves for which $n_r \in [f_3, 1)$ are rejected and the agent stays at its current position $\mathbf{r}_\mu$,

$$f_1\left(\mathbf{r}'_\mu\right) = \begin{cases} 0, \dfrac{f_3}{n_r} \le 1 \\ f_3, \dfrac{f_3}{n_r} > 1 \end{cases}, \forall \mathbf{r}'_\mu \in D^+. \tag{13}$$

From the two cases of D^- and D^+, it follows that $f_1 : D \mapsto [0,1]$. It is instructive to draw on the somewhat unaccustomed concept of *utility* here, as the meaning of f_1 becomes clear if we interpret it as a von Neumann-Morgenstern[33] utility function. The actions taken by agent ϕ_μ due to strategy s_μ (see Appendix A 2) have a probability expressed by the physical constraints of f_3 mapped to q_k. Each specific action and the resultant state $\mathbf{r}'_\mu$ are a concrete realization of the distribution of the states expressed by f_3. As this distribution is optimal within the physical constraints of the current state, the choice of $a_{\mu j}$ and therefore the strategy s_μ are necessarily a best response to the strategies s of all other agents. There is no other strategy s^*_μ that agent ϕ_μ could use to improve its utility, i.e., $f_{1\mu}\left(s_\mu, s\right) \ge f_{1\mu}(s^*_\mu, s)$. If the action does not pay off for the agent, i.e., $f_1 = 0$, it is omitted. The probability that an action is omitted increases the higher f'_2 or the lower U_{GS} is. Therefore, the system is in a Markov perfect equilibrium[34] and the majority charge carriers are in an optimal spatial distribution.

C. Electrode model

In order for the simulation to attain dynamic equilibrium, we need to define electrodes that can create or annihilate agents. The electrode model should also provide a description of the charge-carrier injection process. As an electric current is directly proportional to the applied voltage, a proper electrode model must be a function of the source-drain voltage U_{DS}.

We begin by defining subspaces $C_{S,D}$ that reflect the size and position of the source and drain electrodes in the simulation space C_{sim} of the molecular environment. The local energy of these subspaces is then set to a material-specific work function Φ^M modified by U_{DS},

$$E_L\left(\mathbf{r}\right) = \Phi^M_{S,D} \pm eU_{DS}, \forall \mathbf{r} \in C_{S,D} \subseteq C_{sim}. \tag{14}$$

The injection of charge carriers from the source into the OSC or from the OSC into the drain then reproduces the material properties of the electrodes, their basic geometry, and the operating voltage applied between them.

The definition of the electrodes as subspaces of the simulation space allows them to be included completely in the multi-agent framework. Agents can leave or enter electrode spaces with no other constraints than the utility they gain for doing so. However, with increasing U_{DS}, a certain drift towards the drain electrode is induced by increasing f_1 for actions taken to leave the source or enter the drain.

Not only the energy of the electrodes must be a function of the applied voltage U_{DS}, but especially also the electrode charge. From the capacitor equation in which $A_{S,D}$ is the area of the electrodes and d_{DS} is the distance between them, we calculate the electric charge Q_S of the source electrode as a function of U_{DS} and use this charge to determine an occupation number n_S that reflects the minimum number of agents necessary to represent Q_S. Once n agents have left the source, this target is restored by the creation of n new agents in the source space,

$$\begin{aligned} Q_S &= \varepsilon_0 \varepsilon_r \frac{A_{S,D}}{d_{DS}} U_{DS}, \\ n_s &= \left\lceil \frac{Q_S}{e} \right\rceil, \\ \hat{a}^\dagger &: f\left(U_{DS}\right) \mapsto \left\{\mathbf{r}_{\mu+1\ldots n} \in C_S\right\}. \end{aligned} \tag{15}$$

The target of the drain electrode is defined not to be occupied by agents; so if all K agents of a charge carrier have entered the drain-electrode-space, the agents are removed from the simulation and the counter for transmitted charge N_t is increased by one,

$$\begin{aligned} n_D &= 0, \\ \hat{a} &: f\left(\{1 \ldots \mu \ldots K\} \,|\mathbf{r}_\mu \in C_D\right) \mapsto \emptyset. \end{aligned} \tag{16}$$

III. SIMULATIONS

A. System and setup

In our simulations, we use a system consisting of 25 molecules of C_{60}-functionalized n-octadecyl-phosphonic acid and 75 molecules of n-decyl-phosphonic acid to model the channel of an OFET. This composition reflects the experimental setup with a 30% C_{60} concentration.[7] While the C_{60}-functionalized molecules represent the n-type semiconductor,[10] the non-functionalized molecules act as structural support for the self-assembled monolayer (SAM).[7] Nine snapshots were taken from molecular-dynamics simulations of the system.[7] The time between the snapshots is as short as 1 ps. This short time step was chosen to obtain an estimate of the influence of dynamic disorder on the transmission properties from subsequent calculations.

A semiempirical AM1[25] wavefunction was calculated for each snapshot with the massively parallel EMPIRE[26,27] program. The A_L hypersurfaces were subsequently calculated from these wave-functions with the in-house program VWF2cube[35] on a cubic grid with 0.5 Å spacing.

The optimization of the spatial current distribution is carried out with a custom program (see Appendix A 3) that uses the corresponding routine of the EMPIRE program to calculate the overlaps between agents.

We modelled the dependency of the transmission on U_{DS} and U_{GS}. For the U_{DS}-dependency, we simulated the transmission for a set of voltages $V_{DS} = \{0.25\text{ V}, 0.5\text{ V} \ldots 5.0\text{ V}\}$. For each voltage $U_{DS} \in V_{DS}$, we calculated the transmission for 29 different source-gate voltages $U_{GS} \in V_{GS} = \{0.1\text{ V}, 0.2\text{ V} \ldots 3.0\text{ V}\}$. The simulation was conducted ten times for each pair of (U_{DS}, U_{GS}). At the end of each simulation, the numbers of transmitted charge carriers N_t and of charge carriers in the system N were recorded. The arithmetic mean of N_t and N, respectively, was calculated for each pair of (U_{DS}, U_{GS}) and plotted against U_{GS}. A simulation consists of 10^4 steps and each step of 3×10^3 variation-cycles.

The electric response of the system was modeled by perturbations of the equilibrium caused by changing U_{GS}. For each source-drain voltage $U_{DS} \in V_{DS} = \{0.25\text{ V}, 0.5\text{ V} \ldots 3.0\text{ V}\}$, the source-gate voltage U_{GS} was tuned in steps of $|\Delta U_{GS}| = 0.1$ V through the sequence $V_{GS}^{\updownarrow} = (0.1\text{ V}, 0.2\text{ V} \ldots 3.0\text{ V}, 2.9\text{ V} \ldots 0.0\text{ V})$ in ten consecutive switching-cycles such that ΔU_{GS} perturbs the previous equilibrium. Each calculation of $\left(U_{DS}, V_{GS}^{\updownarrow}\right)$ was performed 50 times and the arithmetic means of N_t and N were calculated for each of the ten switching-cycles. A simulation consists of 10^2 steps and each step of 3×10^2 variation-cycles. The range of the source-drain voltage was extended up to $V_{DS} = \{0.25\text{ V}, 0.5\text{ V} \ldots 4.5\text{ V}\}$ for one snapshot to investigate the system behavior after electric breakdown of the insulating alkyl-chain layer.

An electron was represented by $K = 10$ agents. This number of basis functions has proven to be optimal for our systems; larger K only led to extensive stacking of supporting agents in space, thus increasing the computational effort without changing the charge-carrier distribution. Less agents give correspondingly poorer resolution. Source and drain were modeled as top-contact gold electrodes. The work function of the (100)-plane of gold $\Phi^{\mathrm{Au}(100)} = 5.47$ eV, which is energetically the lowest,[36] was used to adjust the local energy of the electrode subspaces. The simulation space did not comprise the whole SAM but was confined to a space ca. 15% smaller in the x- and z-directions and ca. 25% smaller in the y-direction. This restriction became necessary to avoid ambiguities from the non-periodic calculation of the local energy hypersurface for snapshots from periodic MD-simulations.

B. Results and discussion

Figure 1 shows the number N_t of transmitted electrons under varying U_{GS} for all values of U_{DS} investigated. Transmission sets in for $U_{GS} \approx 0.5$ V and rises steeply to reach a saturation limit at higher U_{GS}-values. For values of $U_{DS} \geq 3.5$ V, an abrupt increase in transmission is found after reaching the saturation limit. From that point on, the curves run a rather flat course and increase of the transmission with higher source-gate-voltages is marginal. Figure 2 shows a snapshot of the agent distribution in the C_{60}-monolayer of the channel at (3.5 V, 2.8 V) and (3.5 V, 2.9 V). Though a certain leakage current[7] is visible

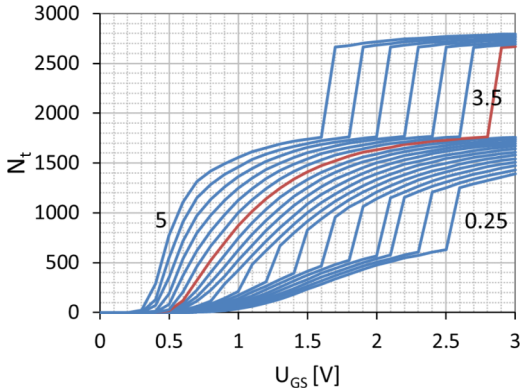

FIG. 1. Number of transmitted electrons, N_t, for different source-drain voltages as a function of the source-gate voltage. The imprinted numbers depict source-drain voltages, which increase from right to left in 0.25 V steps. The red line depicts the lowest source-drain voltage for which an electric breakdown is observed.

for (3.5 V, 2.8 V) especially under the source-electrode, the insulating layer of alkyl-chains is substantially more populated at (3.5 V, 2.9 V). Therefore, we interpret this region as electric breakdown of the system.

Figure 3 shows the number of electrons, N, present in the system under varying U_{GS}. For low source-gate-voltage but high source-drain-voltage, the system charges heavily because of the high utility of leaving the source. The agents' ability to act under these conditions is marginal, and as a result, there is little to no transmission for conditions of peak charge. The threshold voltage of $U_{th} = U_{GS} \approx 0.5$ V becomes apparent from the steep descent of the system charge from $U_{GS} = 0.4$ V $\rightarrow 0.5$ V. For $U_{DS} \leq 3.0$ V, the system charge levels off at $N \approx 4$ and shows only small increase with increasing U_{GS}. The

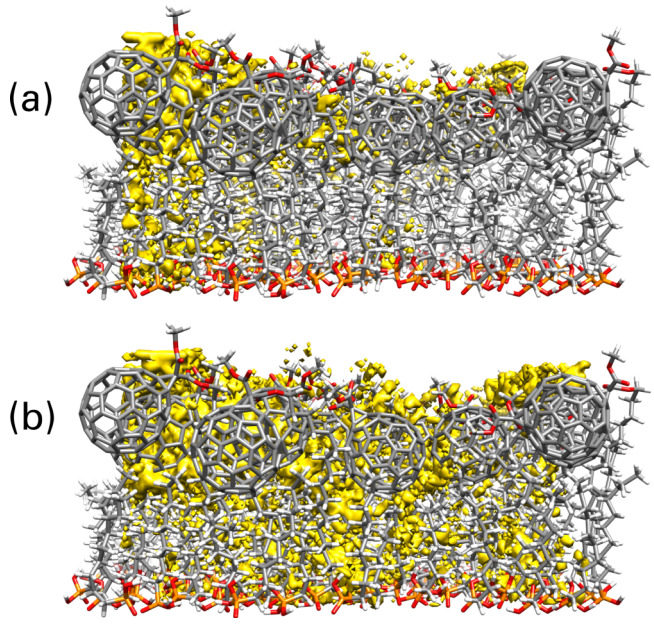

FIG. 2. Snapshot of the agent distribution before (a) and after (b) the electric breakdown at (3.5 V, 2.8 V) and (3.5 V, 2.9 V), respectively. The source-electrode is modeled on top of the C_{60}-layer on the left; the drain-electrode is on the right. While agents spill into the alkyl-layer for (3.5 V, 2.8 V) already, the insulating effect is completely diminished for (3.5 V, 2.9 V).

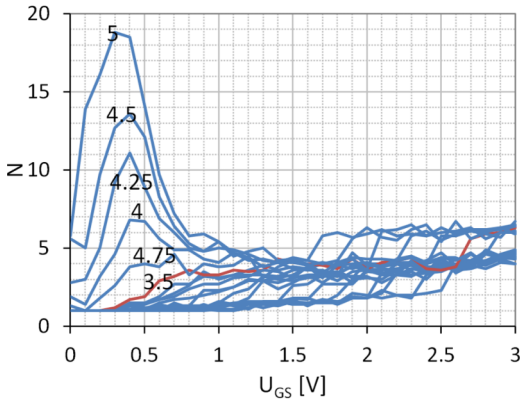

FIG. 3. Number of electrons in the system, N, for different source-drain voltages as a function of the source-gate voltage. The onset of a substantial conduction around 0.5 V can be seen from the strong decrease of the system charge. Imprinted numbers depict source-drain voltages. The red line depicts the lowest source-drain voltage for which an electric breakdown is observed.

electric breakdown is again visible from the abrupt increase in capacitance.

The electric response of the system to changes in U_{GS} is shown in Figure 4 for one snapshot at $U_{DS} = 3.0$ V. Data for all values of U_{DS} are available in the supplementary material.[41] All ten switching-cycles show only little variation in their switch-on (blue) or switch-off (red) curves except for the switch-on sequence of the very first cycle. Changes in system charge or transmission again set in for the threshold voltage of $U_{th} \approx 0.5$ V. Once the first switching cycle is complete, the system begins a new cycle from $N \approx 3$. At the threshold voltage, the system charge first decreases, then rises steeply with increased source-gate-voltage. In the switch-off sequence, the system discharges with a smaller curvature as U_{GS} decreases so that a gap opens between the switch-on and the switch-off sequences of the switching-cycles. Note that the very first switch-on sequence behaves differently: here, the system charges for values of U_{GS} where it discharges in the following switch-on sequences. This behavior is also recognizable in the transmission curves. Transmission sets in at $U_{th} \approx 0.5$ V to stall immediately and then starts to increase again with some delay to the system charge.

To estimate the effect of dynamic disorder, we averaged the system charge over all switching-cycles per snapshot. The plot of the averaged curves in Figure 5 shows that, while the curves converge for lower values of U_{GS}, they diverge strongly for higher values. For $U_{GS} > 1.5$ V, the spread becomes so large that switch-on and switch-off curves become essentially indistinguishable.

A comparison of the two snapshots with the largest divergence shows that the size of the gap between the switch-on and switch-off sequences, the maximum transmission at $U_{GS} = 3.0$ V and its gradient, and the system charge below U_{th} can vary significantly for structures that are only 2 ps apart. Supposing that such structural changes could be caused by operating the transistor, we can draw on the idea of switching the device on in one snapshot (blue solid lines in Figure 5) and switching it off in the other (red solid line). Then, the switching curves would cross and show a second gap. As the

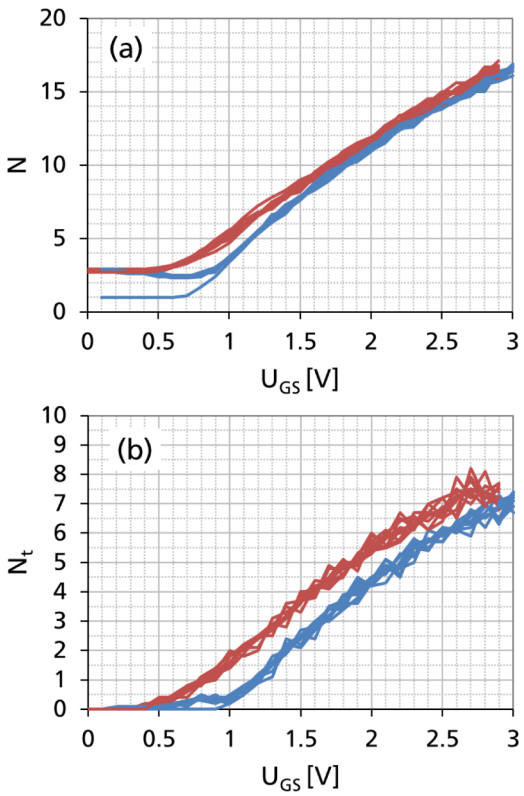

FIG. 4. System charge, N, (a) and transmitted electrons, N_t, (b) for $U_{DS} = 3.0$ V for ten switching-cycles on a single snapshot. Switch-on sequences are shown in blue and switch-off in red. The gap between sequences is due only to electronic effects (*electronic hysteresis*).

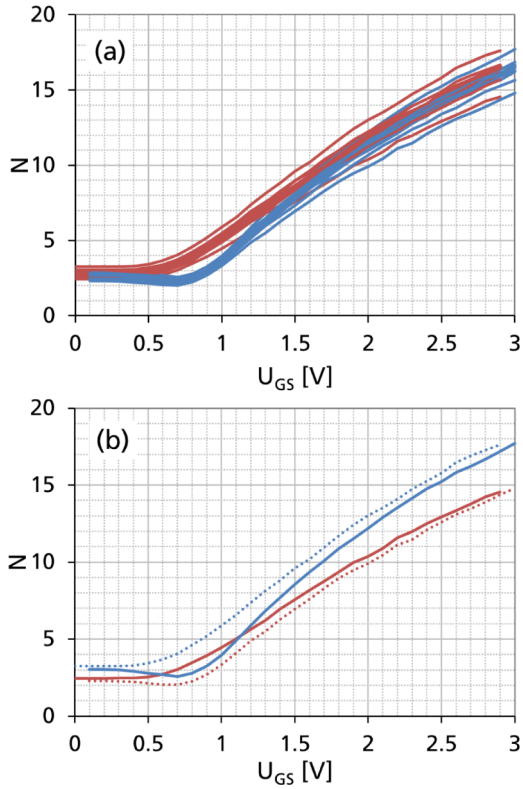

FIG. 5. Overlay of averaged switching cycles for all snapshots showing the effect of dynamic disorder as a spread in the switch-on and switch-off sequences. The effect of electronic hysteresis is visible between 0.5 V and 1.0 V (a). The comparison of the two snapshots with the largest divergence shows an additional gap between the sequences that is due to the different geometries of the snapshots (*structural hysteresis*) (b).

first gap is only due to changes in the electronic transport in a single snapshot, we refer to it as *electronic hysteresis*, while the second gap is due to structural differences between different snapshots and we refer to it as *structural hysteresis*.

While the occurrence of structural hysteresis is straightforward, electronic hysteresis is not. From previous studies of the same system based on an A_L hypersurface[7] and on Landauer theory,[37] we know that we can assume charge transport to take place along paths of favorable energy. The paths form a network through the semiconductor layer as shown in Figure 6. By increasing f_3 via U_{GS}, more and probably shorter pathways become accessible for electrons, enabling them eventually to bypass charge congestions in traps.[38] The different accessible pathways in the A_L-network at different U_{GS} together with temporarily trapped charge carriers change the optimal spatial distribution of the current subject to U_{GS}. These changes in optimality give rise to the seemingly paradoxical[39] situation of momentary decreased capacitance when switching on the transistor.

The method does not include a time scale and therefore does not allow the currents to be calculated. Hence, instead of the conductance, we find the capacitance of the system as a result, and instead of I/V-curves, we give capacitance-curves. As the connection between conductance G and capacitance C is only a reciprocal time, i.e., $G = Ct^{-1}$, the electronic properties of the system should be captured sufficiently by changes in its capacitance.

The capacitance plots (Figs. 1 and 3-5) resemble features of experimental I/V-curves[7] for this system. The simulated threshold voltage of $U_{th} = 0.5$ V agrees well with experiment, from which we infer that our treatments of both charge-carrier mobility and the field-effect are reasonable. The intersection of on/off-curves is in accord with experiment, although the contributions of structural and electronic hysteresis cannot be separated. There is a drain-current drop in the switch-on phase of experimental I/V-curves, which might serve as an indication of electronic hysteresis.

In these simulations, we have used the vacuum work function for the gold electrodes. Experiments,[3,40] however, show the actual work function of gold electrodes in organic systems to be 1–1.5 eV higher than the corresponding vacuum levels. Increasing the source-drain voltage as shown in Figs. 1-3 by this amount, i.e., the simulation for $U_{DS} = 3.0$ V corresponds to an experiment at $U_{DS} = 2.0$ V, improves the agreement between simulation and experiment.

The average spatial charge distribution of ten transport simulations is shown in Figure 7 (Multimedia view). Additionally, snapshots of the evolution of the charge distribution are given in the supplementary material for nine consecutive simulation steps.[41] The working principle of the electrode model is visible from the agents located at the source-electrode space, while the drain-electrode space is nearly empty. A comparison with Figure 6 clearly shows that the charge is distributed in the

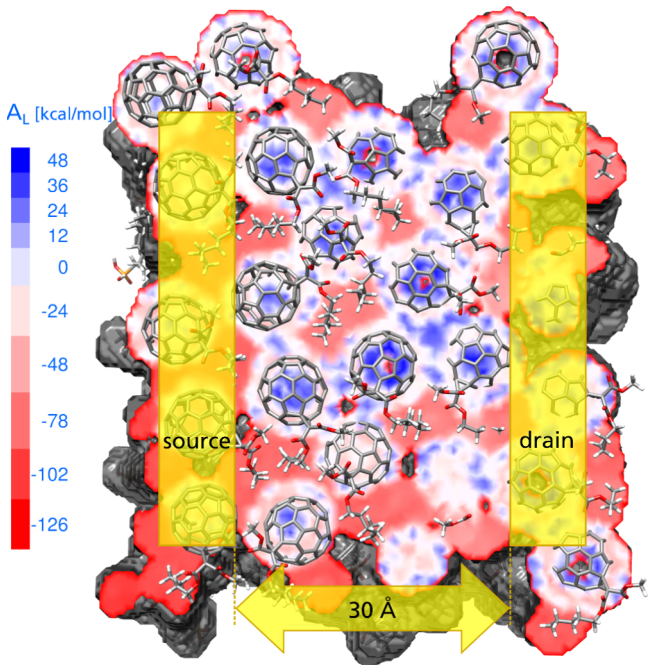

FIG. 6. Horizontal cut through the A_L hypersurface in the region of the C_{60} semiconductor. The insulating effect (red color range) of the alkyl chains is distinguished from the high potential for electron conduction (blue color range). This potential is clearly not limited to individual C_{60} groups but also comprises energy sinks in the space between two or three C_{60} moieties in close proximity. These sinks are a feature of the OFET channel as a whole and as such render hopping between molecules as transport mechanism disputable. Dimension and positions of source and drain electrode modeled in top-contact geometry are shown.

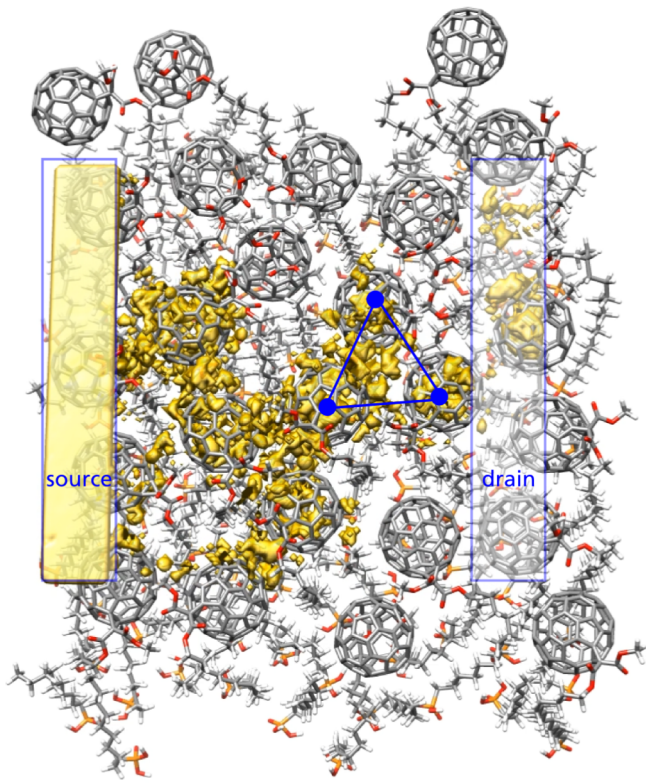

FIG. 7. Average spatial charge distribution of 10 simulation runs for $U_{GS} = 0.8$ V, $U_{DS} = 3.0$ V. The isosurface includes all positions populated on average by at least one agent. The populated source-electrode is visible on the left. Agents are distributed over the whole channel including interstitial energy sinks following the potential shown in Figure 6. The importance of the interstitial regions can be seen from the distribution near the source-electrode, where electron density is largely located in intermolecular sinks, and from the C_{60} triangle near the drain-electrode, where electron density is distributed not only among all fullerenes but also the space between them. (Multimedia view) [URL: http://dx.doi.org/10.1063/1.4927397.1]

regions of high local electron affinity. Transport takes place in these regions, which is consistent with transport simulations[37] based on Landauer theory. The way the charge is distributed over several fullerene moieties and also the space between them does not allow for the definition of clear donor or acceptor regions.

The evolution of the charge distribution during a simulation takes place mainly on the outside surfaces of the fullerenes, as can be seen by the interstitial charge near the source electrode in the lower left area of Figure 7 and the still images in the supplementary material.[41] Interstitial energy sinks have been shown to arise from the intermolecular interaction of fullerenes[38] and seemingly form a network of energetically favorable paths through the channel. In Figure 7, an exemplary interstitial trap in a fullerene-triangle close to the drain is highlighted.

Nonetheless, the propagation of charge carriers continues only when agents become temporarily trapped inside nearby fullerenes. The slice through A_L shown in Figure 6 shows that an energy barrier must be overcome in order to charge or discharge a fullerene on the inside. While this charging and discharging of the fullerenes can be interpreted as hopping, transport on the outside surface is more coherent and band-like. Once charge carriers leave interstitial traps, especially those located near the centers of fullerene-triangles, the charge carriers in the fullerenes become mobile and the fullerenes discharge.

IV. CONCLUSION

A simple multi-agent model for charge transport in n-type semiconductors has been presented, which takes the entire system into account. The derivation is general and can also be applied to p-type semiconductors, in which case the agents correspond to holes. A simple yet effective electrode model has been used to describe charge-carrier injection which implements drift without running into the subtleties of defining an explicit source-drain gradient and naturally allows charge carriers to re-enter the source and leave the drain, respectively. Accounting for the discrepancy between the source-drain voltage of the gold electrode in a vacuum and in an OFET, the model gives realistic descriptions, within experimental uncertainties, of the capacitance behavior. Visualizations of the spatial charge distribution provide an intuitive understanding of OFET operation and are in agreement with different methods and with experimental and theoretical descriptions of material properties. Simulations on several snapshots of the system allow the impact of dynamic disorder on charge transport to be estimated. The phenomenon of hysteresis is explained by structural changes due to dynamic disorder from operating the device and by a destruction of optimality of the transport paths under influence of the gate-field.

The multi-agent model completely avoids the ambiguities in defining Miller-Abrahams attempt-to-hop rates or Marcus theory transfer integrals. Neither charge carriers nor traps are arbitrarily localized in confined spaces. Traps arise naturally from the wave function of the OFET channel geometry from which the E_L potential is calculated. Charge carriers are free to distribute in the potential hypersurface as fits best. The structures of the local energy hypersurfaces show that it is virtually impossible, or at least not reasonable, to define localized donor and acceptor sites in the OFET channel. By taking the whole channel as potential in the multi-agent model, both are not necessary. The agents' constant attempt to optimize energetic utility captures electronic dynamics without the need for an attempt-to-hop rate, and the lack of arbitrarily defined localized states renders the need for transfer integrals between such states unnecessary.

ACKNOWLEDGMENTS

This work was supported by the Cluster of Excellence "Engineering of Advanced Materials" (EXC35) financed by Deutsche Forschungsgemeinschaft (DFG).

APPENDIX: ALGORITHMIC DETAILS

1. Codomain of f_1

If we define by D^- a subset of the domain for which $f_2' \leq f_2$, then $f_3 \geq 1 \forall \mathbf{r}'_\mu \in D^-$, which is meaningless, so the physical probability of accepting a new state in that case is always $q_k = 1$ for all k referring to valid actions. As a result, agents are indifferent over all positions in D^-, which we depict by writing $\mathbf{r}'_{\mu_a} \sim \mathbf{r}'_{\mu_b}$,

$$\begin{gathered} \mathbf{r}'_{\mu_a}, \mathbf{r}'_{\mu_b} \in D^- = \left\{ \mathbf{r}'_\mu \middle| f_2' \leq f_2 \right\} \subseteq D, \\ f_3\left(\mathbf{r}'_\mu\right) \geq 1 \Rightarrow q_k = 1, \forall \mathbf{r}'_\mu \in D^-, \\ f_2'\left(\mathbf{r}'_{\mu_a}\right) \leq f_2'\left(\mathbf{r}'_{\mu_b}\right) \Rightarrow \mathbf{r}'_{\mu_a} \sim \mathbf{r}'_{\mu_b}, \\ f_1\left(\mathbf{r}'_\mu\right) = 1, \forall \mathbf{r}'_\mu \in D^-. \end{gathered} \tag{A1}$$

If we define in a similar manner a subset D^+ for which $f_2' > f_2$, then the physical probability of accepting a new state is expressed directly by f_3, and as a result, agents have a preference for states of lower energy over states of higher energy. We depict this preference with $\mathbf{r}'_{\mu_m} \succ \mathbf{r}'_{\mu_n}$,

$$\begin{gathered} \mathbf{r}'_{\mu_m}, \mathbf{r}'_{\mu_n} \in D^+ = \left\{ \mathbf{r}'_\mu \middle| f_2' > f_2 \right\} \subseteq D, \\ f_3\left(\mathbf{r}'_\mu\right) \mapsto]0,1[\Rightarrow q_k = f_3, \forall \mathbf{r}'_\mu \in D^+, \\ f_2'\left(\mathbf{r}'_{\mu_m}\right) < f_2'\left(\mathbf{r}'_{\mu_n}\right) \Rightarrow \mathbf{r}'_{\mu_m} \succ \mathbf{r}'_{\mu_n}. \end{gathered} \tag{A2}$$

The indifference over states in the case of D^- and the preference over low energy states in the case of D^+ give rise to an ordering of states in the domain that is numerically expressed by f_1, which maps the domain to the closed interval $[0,1]$,

$$\begin{gathered} f_1\left(\mathbf{r}'_{\mu_a}\right) = f_1\left(\mathbf{r}'_{\mu_b}\right) > f_1\left(\mathbf{r}'_{\mu_m}\right) > f_1\left(\mathbf{r}'_{\mu_n}\right), \\ \mathbf{r}'_{\mu_a} \sim \mathbf{r}'_{\mu_b} \succ \mathbf{r}'_{\mu_m} \succ \mathbf{r}'_{\mu_n}, \\ f_1 : D \mapsto [0,1]. \end{gathered} \tag{A3}$$

2. Markov strategies

The chain of all actions can be combined into the history h' of the current state ρ' of the system, where in starting state ρ^0, an action a^0 is taken that leads to state ρ^1 and so on,

$$h' = \left(\rho^0, a^0, \rho^1, a^1, \ldots \rho'^{-1}, \rho'\right). \tag{A4}$$

We can define a behavioral strategy s_μ for the agents from the history of the current state.[34] s_μ gives the probability that agent ϕ_μ takes action $a_{\mu j}$ for history h', with $j \in \{1,2\ldots\#A\}$ and $\#A$ being the cardinality of A. As an agent cannot anticipate the actions of other agents, the energetic environment for each agent is inherently uncertain. Therefore, an agent's action can only be based on the current state of the system, not its entire history or its probable future states. This constraint means that the chain of all actions leading to ρ' is a Markov chain and is met by realizing that a state ρ' can be reached from different histories h'_1 and h'_2 so that $\rho'_1 = \rho'_2 = \rho'$. We can then define the problem of charge transport through an organic semiconductor as a Markov decision problem of occupying optimal states in the domain using Markov strategy s_μ,

$$s_\mu\left(h'_1, a_{\mu_j}\right) = s_\mu\left(h'_2, a_{\mu_j}\right). \tag{A5}$$

3. Multiagent quantum Monte Carlo program

Pseudo-code of the multi-agent software used to model the spatial charge distribution.

MAQM program
! Initialization:
$D \leftarrow C_{sim}$
$E_L(\forall \mathbf{r} \in C_{S,D}) \leftarrow \Phi^{\mathrm{M}}_{S,D} \pm eU_{DS}$
Calculate n_S
! Simulation steps:
repeat
  ! Variation-cycles:
  repeat
    field $\leftarrow \forall \mathbf{r}_\mu$
      forall $i \in N$ **do**
        forall $\phi_\mu \in K$ **do**
          Randomly select $a \in A | \mathbf{r}'_\mu \in D$
          Calculate f_2, f'_2 using *field*
          if $f_1 \neq 0$ **then**
            $\mathbf{r}_\mu \leftarrow \mathbf{r}'_\mu$
  until max number of cycles reached
  Adjust n_S, n_D
until max number of steps reached

[1]J. Cornil, S. Verlaak, N. Martinelli, A. Mityashin, Y. Olivier, T. Van Regemorter, G. D'Avino, L. Muccioli, C. Zannoni, F. Castet, D. Beljonne, and P. Heremans, Acc. Chem. Res. **46**, 434 (2013).
[2]R. Noriega and A. Salleo, in *Charge Transport Theories in Organic Semiconductors*, edited by H. Klauk (Wiley-VCH, Weinheim, 2012).
[3]H. Bässler and A. Köhler, in *Unimolecular and Supramolecular Electronics I*, edited by R. M. Metzger (Springer, Berlin, Heidelberg, 2012).
[4]R. A. Marcus and N. Sutin, Biochim. Biophys. Acta **811**, 265 (1985).
[5]A. Miller and E. Abrahams, Phys. Rev. **120**, 745 (1960).
[6]M. Novak, A. Ebel, T. Meyer-Friedrichsen, A. Jedaa, B. F. Vieweg, G. Yang, K. Voitchovsky, F. Stellacci, E. Spiecker, A. Hirsch, and M. Halik, Nano Lett. **11**, 156 (2011).
[7]C. M. Jager, T. Schmaltz, M. Novak, A. Khassanov, A. Vorobiev, M. Hennemann, A. Krause, H. Dietrich, D. Zahn, A. Hirsch, M. Halik, and T. Clark, J. Am. Chem. Soc. **135**, 4893 (2013).
[8]J. E. Anthony, A. Facchetti, M. Heeney, S. R. Marder, and X. Zhan, Adv. Mater. **22**, 3876 (2010).
[9]M. Halik, H. Klauk, U. Zschieschang, G. Schmid, C. Dehm, M. Schutz, S. Maisch, F. Effenberger, M. Brunnbauer, and F. Stellacci, Nature **431**, 963 (2004).
[10]M. Novak, C. M. Jäger, A. Rumpel, H. Kropp, W. Peukert, T. Clark, and M. Halik, Org. Electron. **11**, 1476 (2010).
[11]T. Schmaltz, A. Y. Amin, A. Khassanov, T. Meyer-Friedrichsen, H. G. Steinruck, A. Magerl, J. J. Segura, K. Voitchovsky, F. Stellacci, and M. Halik, Adv. Mater. **25**, 4511 (2013).
[12]J. Tsurumi, A. Y. Amin, T. Okamoto, C. Mitsui, K. Takimiya, H. Matsui, M. Halik, and J. Takeya, Org. Electron. **15**, 1184 (2014).
[13]T. Schmaltz, A. Krause, S. Leitherer, C. Jäger, T. Bauer, M. Thoss, T. Clark, and M. Halik, "Correlation between chemical structure, morphology and electrical properties of benzothieno[3,2-b][1]benzothiophene-based self-assembled monolayers for transitor applications" (unpublished).
[14]N. Ehrentreich, *The Santa Fe Institute Artificial Stock Market Model Revisited* (Springer, Berlin, Heidelberg, 2008).
[15]B. Chen and H. Cheng, IEEE Trans. Intell. Transp. Syst. **11**, 485 (2010).
[16]E. Bonabeau, Proc. Natl. Acad. Sci. U. S. A. **99** (Suppl. 3), 7280 (2002).
[17]N. R. Jennings, Artif. Intell. **117**, 277 (2000).
[18]T. Clark, K. G. Byler, and M. J. de Groot, *Biological Communication via Molecular Surfaces, Proceedings of the International Beilstein Workshop* (Logos Verlag, Berlin, 2008).
[19]P. Sjoberg, J. S. Murray, T. Brinck, and P. Politzer, Can. J. Chem. **68**, 1440 (1990).
[20]P. Politzer, J. S. Murray, and F. A. Bulat, J. Mol. Model. **16**, 1731 (2010).
[21]B. Ehresmann, B. Martin, A. H. Horn, and T. Clark, J. Mol. Model. **9**, 342 (2003).
[22]T. Clark, J. Mol. Model. **16**, 1231 (2010).
[23]C. Atienza, N. Martin, M. Wielopolski, N. Haworth, T. Clark, and D. M. Guldi, Chem. Commun. **2006**, 3202.
[24]M. Kriebel, D. Sharapa, and T. Clark, "Quantum dynamics on local-property hypersurfaces" (unpublished).
[25]M. Dewar, E. Zoebisch, E. Healy, and J. Stewart, J. Am. Chem. Soc. **107**, 3902 (1985).
[26]M. Hennemann and T. Clark, EMPIRE, Universität Erlangen-Nürnberg & Cepos InSilico GmbH, Erlangen, 2013; see http://www.ceposinsilico.de.
[27]M. Hennemann and T. Clark, J. Mol. Model. **20**, 2331 (2014).
[28]M. J. S. Dewar and W. Thiel, Theor. Chim. Acta **46**, 89 (1977).
[29]M. J. S. Dewar and W. Thiel, J. Am. Chem. Soc. **99**, 4899 (1977).
[30]J. A. Pople and D. L. Beveridge, *Approximate Molecular Orbital Theory* (McGraw-Hill, New York, 1970).
[31]A. Szabo and N. S. Ostlund, *Modern Quantum Chemistry* (Dover Publications, Inc., Mineola, NY, 1996).
[32]N. Metropolis, A. W. Rosenbluth, M. N. Rosenbluth, A. H. Teller, and E. Teller, J. Chem. Phys. **21**, 1087 (1953).
[33]J. von Neumann and O. Morgenstern, *Theory of Games and Economic Behavior*, 3rd ed. (Princeton University Press, Princeton, 1953).
[34]Y. Shoham and K. Leyton-Brown, *Multiagent Systems* (Cambridge University Press, New York, 2009).
[35]M. Hennemann, A. Elkerdawy, and T. Clark, VWF2cube, Universität Erlangen-Nürnberg & Cepos InSilico GmbH, Erlangen, 2013; see http://www.ceposinsilico.de.
[36]*CRC Handbook of Chemistry and Physics*, 93rd ed., edited by W. M. Haynes (Taylor and Francis Group, 2013), see online at http://www.hbcpnetbase.com.
[37]S. Leitherer, C. M. Jager, M. Halik, T. Clark, and M. Thoss, J. Chem. Phys. **140**, 204702 (2014).
[38]T. E. Shubina, D. I. Sharapa, C. Schubert, D. Zahn, M. Halik, P. A. Keller, S. G. Pyne, S. Jennepalli, D. M. Guldi, and T. Clark, J. Am. Chem. Soc. **136**, 10890 (2014).
[39]D. Braess, Unternehmensforschung **12**, 258 (1968).
[40]N. Koch, A. Elschner, R. L. Johnson, and J. P. Rabe, Appl. Surf. Sci. **244**, 593 (2005).
[41]See supplementary material at http://dx.doi.org/10.1063/1.4927397 for capacitance plots covering the whole range of source-drain voltage, images of the evolution of the agent distribution in a simulation run, and images of the structure of the OFET channel.